Journal of Robotics and Control (JRC)
Volume 3, Issue 4, July 2022
ISSN: 2715-5072, DOI: 10.18196/jrc.v3i4.14742

Design and Motion Planning of a Wheeled Type Pipeline Inspection Robot

Rajendran Sugin Elankavi [1], D. Dinakaran [2*], Arockia Selvakumar Arockia Doss [3], R.M. Kuppan Chetty [4], M. M. Ramya [5]
[1, 2, 4, 5] Centre for Automation and Robotics (ANRO), School of Mechanical Sciences, Hindustan Institute of Technology and Science, Chennai, Tamil Nadu, India
[3] School of Mechanical Engineering, Vellore Institute of Technology, Chennai, Tamil Nadu, India
Email: [1] rs.ser0819@hindustanuniv.ac.in, [2] dinakaran@hindustanuniv.ac.in, [3] kuppanc@hindustanuniv.ac.in, [4] mmramya@hindustanuniv.ac.in, [5] arockia.selvakumar@vit.ac.in
*Corresponding Author

***Abstract*— The most popular method for transporting fluids, and gases is through pipelines. For them to work correctly, regular inspection is necessary. Humans must enter potentially dangerous environments to inspect pipelines. As a result, pipeline robots came into existence. These robots aid in pipeline inspection, protecting numerous people from harm. Despite numerous improvements, pipeline robots still have several limitations. This paper presents the design and motion planning of a wheeled type pipeline inspection robot that can inspect pipelines having an inner diameter between 250 mm to 350 mm. The traditional wheeled robot design has three wheels fixed symmetrically at a 120° angle apart from each other. When maneuvering through a curved pipeline, this robot encounters motion singularity. The proposed robot fixes the wheels at different angles to address this issue, allowing the robot to stay in constant contact with the pipe's surface. Motion analysis is done for the proposed and existing robot design to study their behavior inside the pipeline. The result shows that the proposed robot avoids motion singularity and improves mobility inside pipelines. 3d printing technology aids in the development of the proposed robot. The experimental tests on the developed robot inside a 300 mm-diameter straight and curved pipeline show that the robot avoids motion singularity.**

Keywords*— *Inspection robot; Motion singularity; Optimal design; Pipeline robot; Mobile robot

I. INTRODUCTION

Fluids and gases are transported through pipelines, becoming the most popular mode of transportation. Thus, continuous pipeline monitoring is essential to ensure its health and safety [1]. Various methods are available, including visual testing, radiographic testing, ultrasonic testing and hydrostatic testing, the most commonly used Non-Destructive Testing (NDT) inspection methods [2]. However, due to the technological advantages in robotics in the recent decade, they have become the better option. Robots are a better option as entering a small pipeline is difficult for humans [3]. In recent years many developments have been made in In-Pipe Inspection Robot (IPIR) and are grouped under their different locomotion types. They are namely the Pipeline Inspection Gauge (PIG) [4]–[10], screw [11]–[17], inchworm [18]–[24], wall press [25]–[29], walking [30]–[34], caterpillar [35]–[39] and wheel type [40], [41], [50]–[52], [42]–[49] as shown in Fig. 1. These commonly used locomotion types have limitations and advantages [53].

A. *Types of IPIR*

The PIG type uses the water pressure to move inside pipelines and can be used for long-distance [4]–[8]. The screw-type moves in helical motion and does not damage the inner surface of the pipelines [11]–[15]. The inchworm type has less traction and good gripping force, which helps it move inside pipelines [18]–[22]. The wall press type uses the contact force to pass through the pipelines steadily [25]–[29]. The walking type has a complicated mechanism and uses legs to walk, resulting in less slippage and damage to the pipeline's surface [30]–[34]. Caterpillar types move inside pipelines

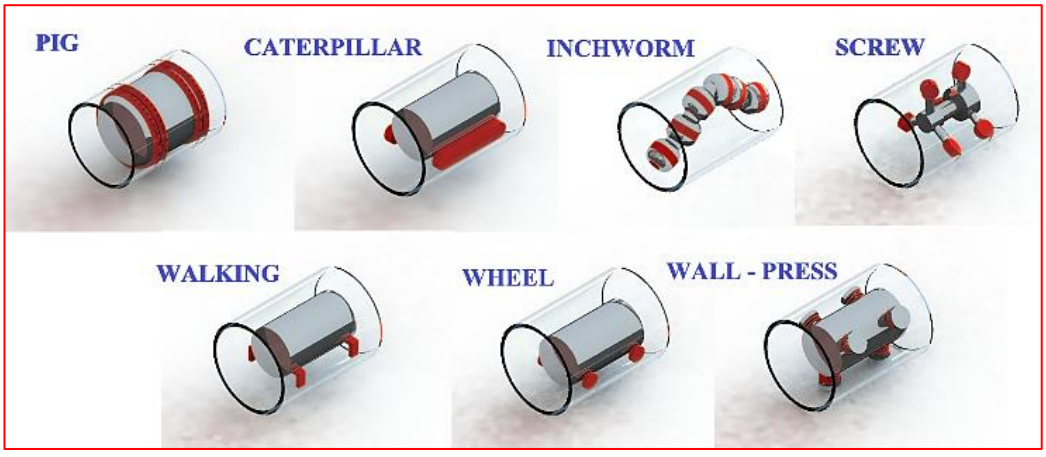

Fig. 1. Different In-Pipe Inspection Robots [62]

using tracked wheels, and its mechanism helps it adapt to inner pipeline conditions [35]–[39]. The wheel type uses the basic rotation of wheels to move inside pipelines and has high mobility compared to the other types [40]–[44]. These robots face many challenges inside the pipeline since it has to pass through curved and branched pipes. While doing so, it faces motion singularity and Irregular motion.

B. Motion Singularity

The loss of contact between the robot and the pipeline junctions like curved pipes, L and T-branch pipes is called "Motion Singularity" [54], [55]. The caterpillar robot provides more stability and is the most commonly used IPIR because of its strong traction force and contact area. It uses tracked wheel to make sure that, regardless of the pipeline's turning angle, it is still in contact with the inner surface [35]–[39]. Steering inside L and T-branch pipes is not easy for this robot [54], [55]. It fails to move through these pipes if one of the wheels loses contact with the pipeline's inner surface causing motion singularity [54].

Fig. 2 shows a caterpillar robot using two modules in place of one to avoid motion singularity while moving in T-branch pipes. The first module mounts three caterpillar wheels at an angle of 120° apart from each other, and in relation to the front module, the second module is infix at 60 degrees [54]. During turning at Y and T-branch pipes, "FAMPER", a pipeline exploration robot, loses contact with the inner surface of the pipeline and causes motion singularity. To overcome the loss of contact, caterpillar wheels were not fixed straight, but rather at an angle of 5 degrees with respect to the robot body. As a result, motion singularity is avoided [55]. In [56], a two-wheel chain robot, which avoids the motion singularity while turning, is presented.

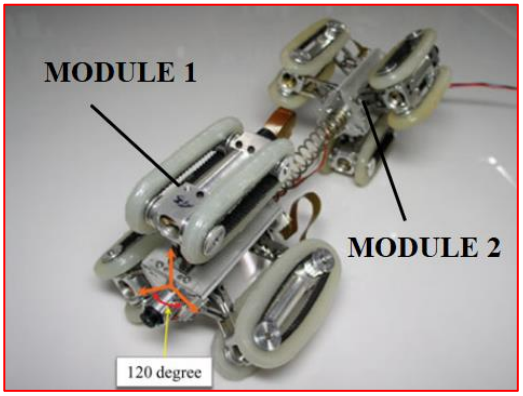

Fig. 2. Two-Module Collaborative Indoor Pipeline Inspection Robot [54]

C. Irregular Motion

Literature shows that many traditional wheeled-type robots have wheels that are symmetrically placed at a 120° angle to ensure uniform loading and better stability during locomotion inside the pipeline. The wheeled robots use the wall press feature to gain this stability [35], [54], [57]–[59]. In [41], Due to the three-wheel configuration in wheeled IPIR, an irregular motion occurs along the circumferential axis of the pipeline in forwarding motion, and the use of six wheels solves the issue.

The wheeled robot having a three-wheel configuration uses two types of wheels to manoeuvre inside the pipelines. According to the Fig. 3, one uses single wheels, and the other uses double wheels.

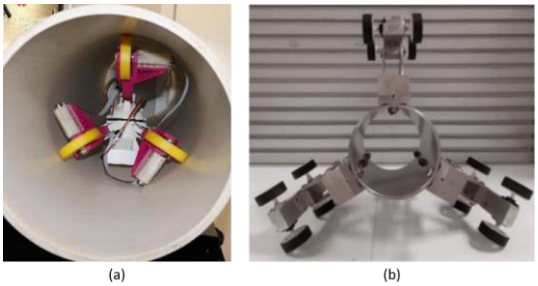

Fig. 3. Prototypes of wheeled robots. (a) Single three-wheel configuration robot [42] and (b) Double three-wheel configuration robot [57]

The Single three-wheel configuration robot tries to rotate along the circumferential direction of the pipeline when it moves forward [60] as shown in the Fig. 4.

Fig. 4. Motion of the robot inside a straight pipeline [60]

The studies related to their motion are limited to straight pipelines. In cases [61], when the robot tries to manoeuvre through the curved pipeline. The robot tries to roll over and thus the orientation of the robot at the finishing end is different compared to the starting end as shown in the Fig. 5. Additionally, the positioning of the wheels makes steering inside branched pipes difficult.

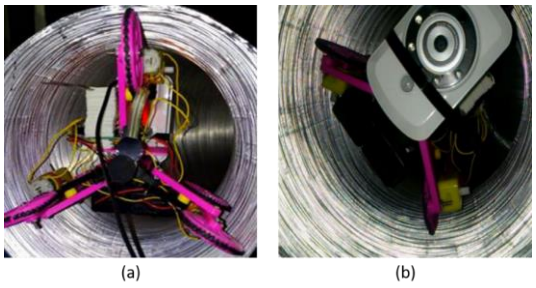

Fig. 5. Orientation of the robot (a) Before entering the curved pipeline and (b) After exiting the curved pipeline [61]

Therefore, this paper focuses on designing a wheeled IPIR using the single three-wheel configuration that could neglect motion singularity and irregular motion while maintaining the same orientation before and after entering the curved pipeline.

D. Contribution

In this paper, a wheeled type IPIR is designed and developed to solve the issue of irregular motion and motion singularity occurring in pipelines. This robot is unique because it has wheels that are not fixed at a 120-degree angle from one another like those on traditional robots. This placement of wheels prevents the robot from rolling over when passing through the curved pipeline and ensures the wheels of the robot are in contact with the pipe surface in any

environment. It also helps the robot to steer inside branched pipes. The traditional robot design is not

The robot is designed using Solidworks software. Simulations are carried out using ADAMS software to test the motion of the designed robot inside curved pipelines. Experiments are conducted inside a 300 mm inner diameter pipeline to observe its motion.

The following is the outline of this article. Section 2 talks about the methods used in this research. Section 3 analyses the motion singularity region inside the curved pipeline for traditional wheeled type robots and proposes a solution. Section 4 discusses the development of the prototype. Section 5 observes the robot's motion inside a straight and curved pipeline and verifies the avoidance of motion singularity. Section 6 concludes the research with future research directions.

II. METHODS

The methodology consists of the following steps as shown in Fig. 6. Initially we design the robot using solidworks. The designed model is exported to ADAMS. Motion analysis is done for the robot using the constraints mentioned in the flowchart. Finally, the results are discussed.

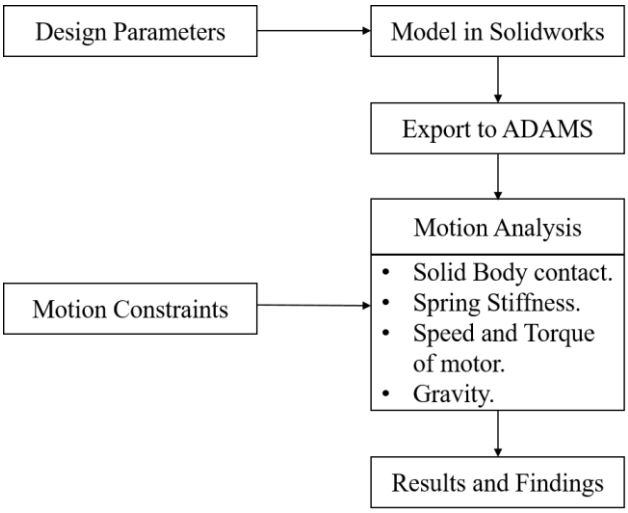

Fig. 6. Research method flowchart

Fig. 7 shows the Solidworks model of the robot. The proposed robot has links, wheels, clamps, a central shaft, legs, spring, fixed joint and prismatic joint. The legs provide better stability inside pipelines. The tiny links serve as the legs' supports. The clamps ensure that all the components remain in their proper places. The wheels are for improving mobility inside pipelines. The central shaft is the main body where all the modular components are attached. The fixed joint doesn't move, and the prismatic joint is the movable joint that gives the necessary force for the wheels to have contact with the inner surface of the pipeline. The required force for the prismatic joint is given by springs which compress and expand based on the pipeline's inner circumference. The robot's design accommodates an internal pipeline diameter of 250 mm to 350 mm.

Fig. 7. Rendered solid model of Robot

The robot mechanism consists of a four-link structure, as shown in Fig. 8. It consists of one prismatic joint and three revolute joints. These joints give the robot more stability as it moves through the pipelines by compressing and extending the legs. It assists the robot in meeting different pipeline situations such as curved or T-branch pipes. To determine the actuator scale, static analysis is performed. The virtual work principle is applied to the free body diagram shown in Fig. 8. Which gives,

$$\partial w = F_{NZ}\,\partial z - F_{SX}\,\partial x = 0 \quad (1)$$

where F_{SX} is the spring force.

The corresponding displacements due to these forces are expressed as,

$$z = 3\ell \sin\theta,\ x = -3\ell \cos\theta \quad (2)$$

Substituting (2) into (1) gives,

$$\partial w = F_{NZ}\,\partial\,(3\ell \sin\theta) - F_{SX}\,\partial\,(-3\ell \cos\theta)$$

$$= F_{NZ} * 3\ell \cos\theta - F_{SX} * 3\ell \sin\theta = 0 \quad (3)$$

Rearranging (3), The spring force F_{SX} at the prismatic joint is related to the normal force F_{NZ} by

$$F_{NZ} = F_{SX} * tan\,\theta \quad (4)$$

The total weight of the robot "W" is equal to the number of the six traction forces acting on the wheel. As a result, each traction force F_{NX} is one-sixth of the whole robot's weight.

$$F_{NX} = W/6 \quad (5)$$

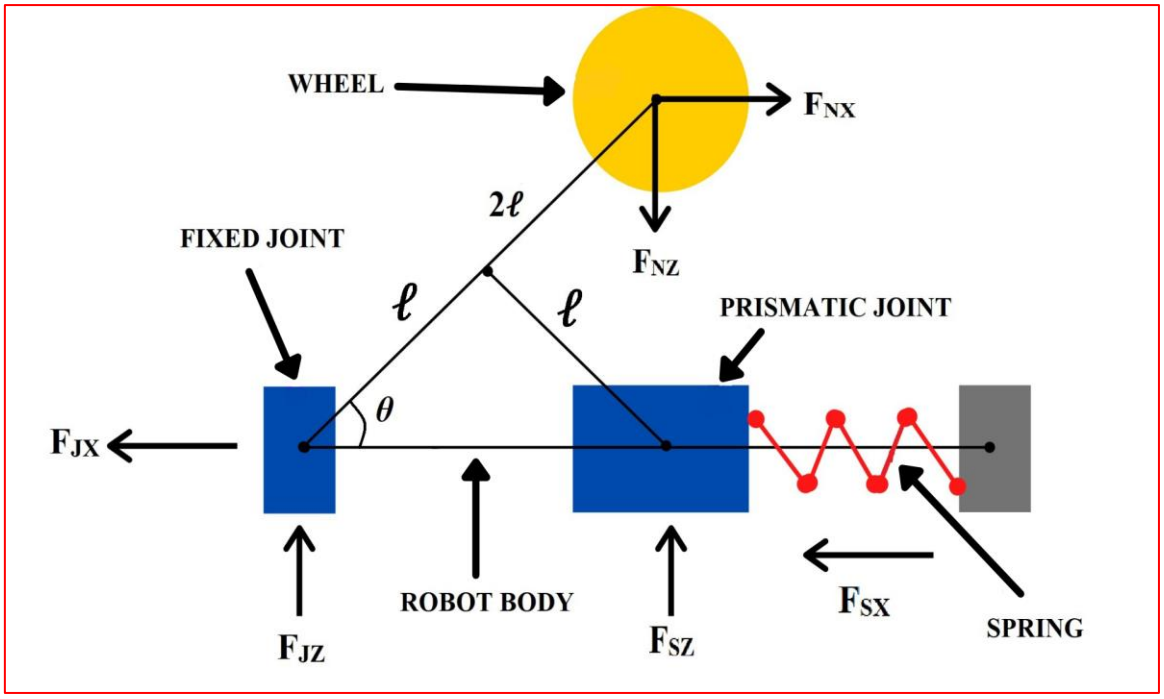

Fig. 8. Free body diagram of the mechanism

The size of the actuator bounded in the wheel is calculated by,

$$\tau = F_{NX} * r = W * r / 6 \quad (6)$$

where r is the radius of the wheel. The above analysis revealed that the robot's weight does not affect the linkage mechanism. This is because the spring force supports the reaction force F_{NZ}. The spring force F_{SX} is shown to be a part of the reaction force F_{NZ} and the reaction forces F_{JX}, F_{JZ} at the fixed joint. Since the robot is 3D printed, it is lighter and thus reduces the torque needed. Thus, the spring stiffness is found to be 2.826 N/mm and it was concluded that the minimum torque required is 5.6 kg-cm. Hence, a decision was taken to use four actuators at the bottom part of the robot with a torque of 2.9 kg-cm each with a total of 11.6 kg-cm.

III. ANALYSIS

ADAMS software carries out the motion analysis. The robot design is imported from Solidworks, and the boundary conditions for the simulation are given in ADAMS software. The conditions used are the spring stiffness, motor rpm and body-to-body contact. The simulations are carried out for the proposed robot and the conditions where the wheels are mounted at 120° apart. In the simulation, the robot first enters a 350mm inner diameter pipeline. After it travels 600 mm, there is a change in the inner diameter of the pipeline, which decreases up to 10 mm, which is 340mm. This change in diameter checks the robot's adaptability for varying diameter pipelines. Then the robot again goes through a straight pipe and meets a curved elbow of 90°. After exiting the curved pipe, it again enters the straight pipe and comes out of the pipeline, as shown in Fig. 9. This simulation environment verifies the robot's ability to pass through straight, curved and varying diameter pipelines.

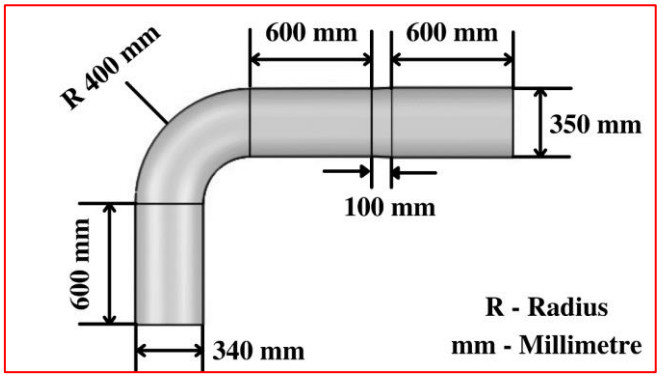

Fig. 9. Dimensions of the pipeline used in the simulation

In both simulations, the parameters used are the same except for the wheel mounting angle. The parameters the robot needs to pass through the pipelines are gravity, motor speed, solid body contact and spring stiffness. The two wheels at the bottom for the front side of the robot are active, and the third wheel acts as a supporting wheel. The three wheels at the backside of the robot are not active. The spring stiffness is 2.826 N/mm, and the motor speed is 100 rpm.

A. Wheeled In-Pipe Inspection Robot

The wheels on traditional wheeled IPIRs are at a 120° angle apart from each other. The angle is measured from the centre point of one wheel to another with respect to the centre axis of the robot body. Fig. 10 shows the simulation environment and parameters.

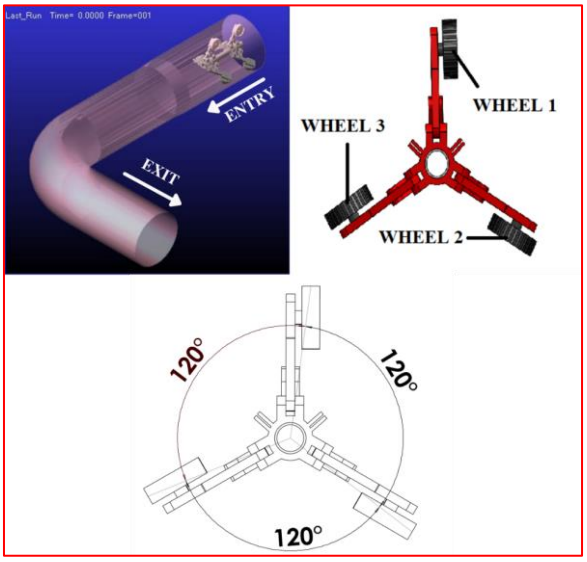

Fig. 10. Simulation environment and parameters used for Wheeled IPIR

Fig. 11 shows the simulation result, and it shows that the robot wheels lose contact while passing through the concave part of the pipeline. The motion singularity occurs because of the uniformed wheel mounting angle. The three legs compress equally as they move through the pipeline because they are connected by a prismatic joint. Thus, causing motion singularity inside curved pipes.

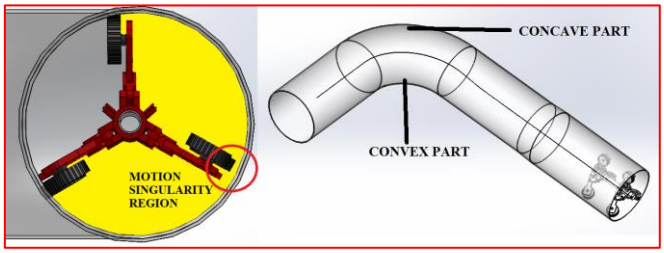

Fig. 11. Singularity region in concave and convex part of the curved pipeline

Fig. 12 shows that when the robot travels inside the straight pipeline of 350 mm. The angular velocity of wheel 1 increases while wheel 2 and wheel 3 remain constant. When the pipe's inner diameter decreases, the three wheels' angular velocity remains constant. Then, when the robot tries to enter the curved pipeline, wheel 3 loses contact, preventing the robot from passing through the curved pipeline. It shows that the angular velocity of wheel 3 has no change in magnitude, which should have been high as it passes the concave part of the pipe. Thus, showing that it lost contact with the pipe wall.

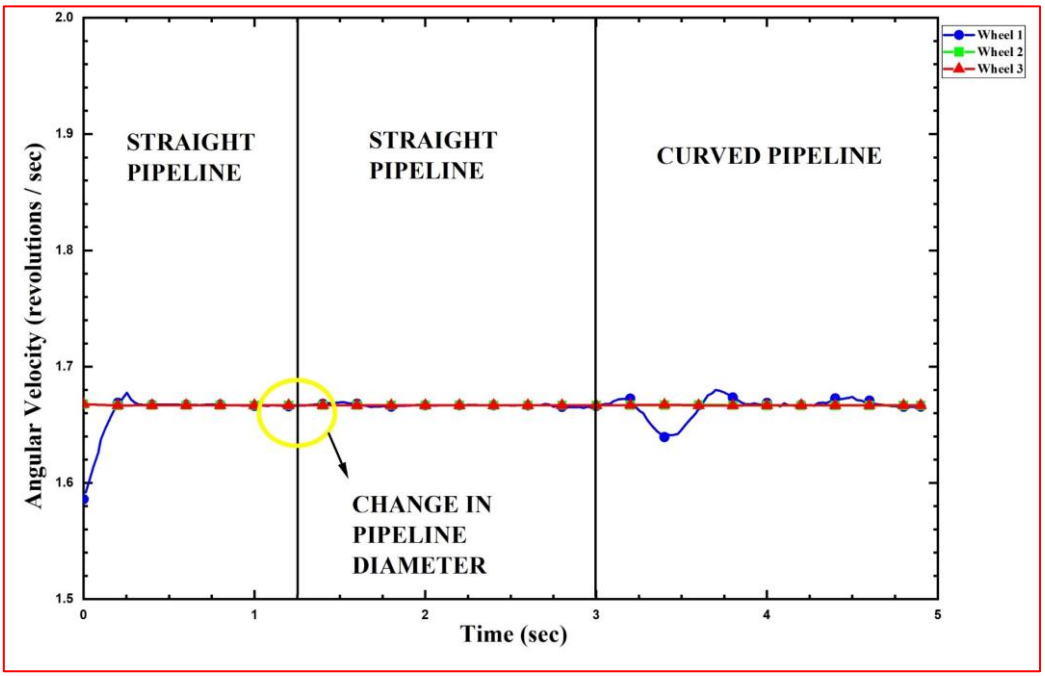

Fig. 12. Angular velocity of wheels when travelling in straight, curved and varying diameter pipeline

Fig. 13 shows the forces applied on wheels when travelling inside the pipeline. When the robot passes through a 350 mm pipeline, wheels 1, 2 and 3 experience a maximum force of about 11.25 N. When the pipeline diameter changes to 340 mm, the maximum force is experienced by wheels 1 and 2 compared to wheel 3, where forces acting on it declines. Then all the forces acting on the wheels become constant. When the robot enters the curved pipeline, the force acting on wheel 3 increases because the wheel loses contact with the concave part of the inner pipeline surface. The high spike in wheel 3 after losing contact is because of the following reason: when the robot tries to pass through a curved pipe, it losses contact with one of the wheels and thus could not pass through but the two wheels that are in contact exerts a force on the spring. As a result of the spring force, the wheels drive the robot backward, causing wheel 3 to collide with the pipe's internal surface, causing a significant force spike.

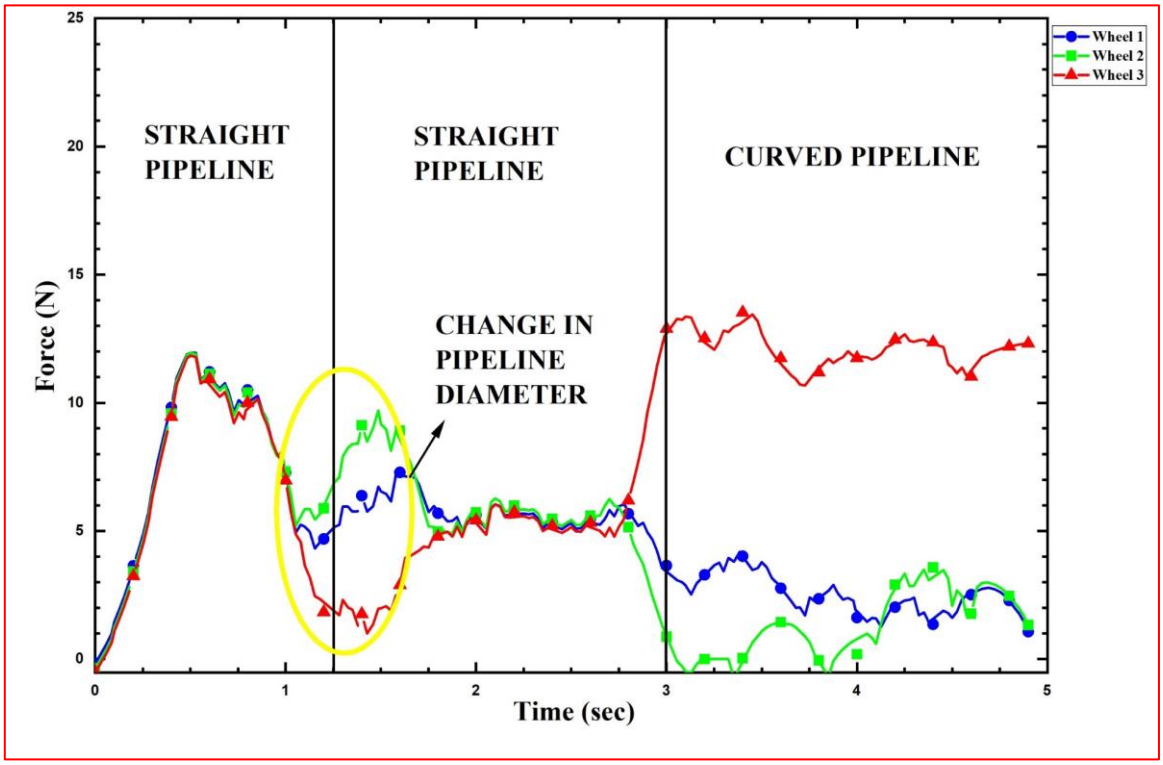

Fig. 13. Force acting on wheels of the robot when travelling in straight, curved and varying diameter pipeline

Fig. 14 shows the spring force when the robot passes through the pipeline. Here, spring 1 denotes the spring in the front, and spring 2 denotes the spring at the back of the robot. The force provided by springs 1 and 2 varies from 1.25 to 12.5 N when the robot passes through a 350 mm inner diameter pipeline. The force exerted by springs 1 and 2 approaches 17.5 N when the inner pipeline diameter increases to 340 mm. When the robot entered the curved pipeline, due to motion singularity, it could not pass; thus, the force in spring 1 reduces. As a result of motion singularity, the back part, due to the inertia of motion, gives a little push at that moment. Thus, the legs on the robot's backside compress, creating a high force of about 25 N at that instant and then decreasing gradually.

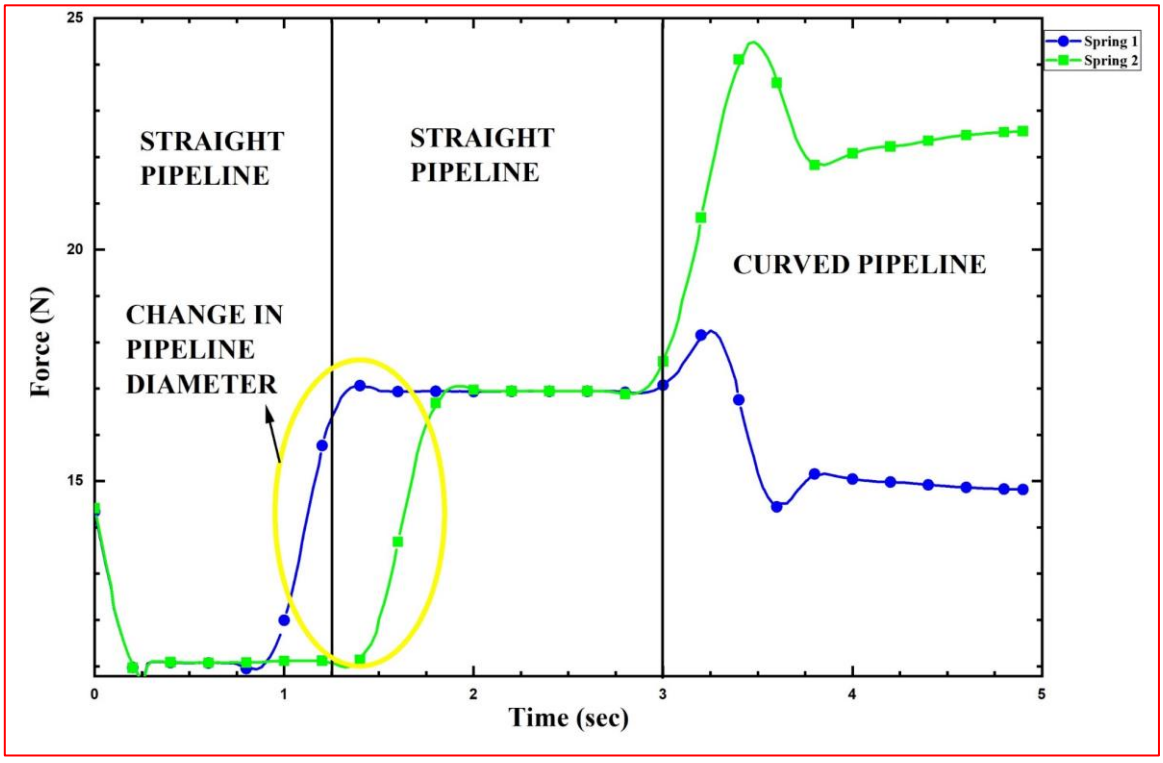

Fig. 14. Spring force of the robot when travelling in straight, curved and varying diameter pipeline

Fig. 15 shows the linear velocity of the robot when travelling inside the pipeline. When travelling inside the straight pipeline of diameter 350 mm, it has an average linear velocity of 0.35 m/s. When the inner diameter of the pipeline decreases to 340 mm, the linear velocity of the robot ranges between 0.30 – 0.35 m/s. Then the robot tries to enter the curved pipeline, and due to motion singularity, it could not pass through it, showing a sweeping decrease in the linear velocity.

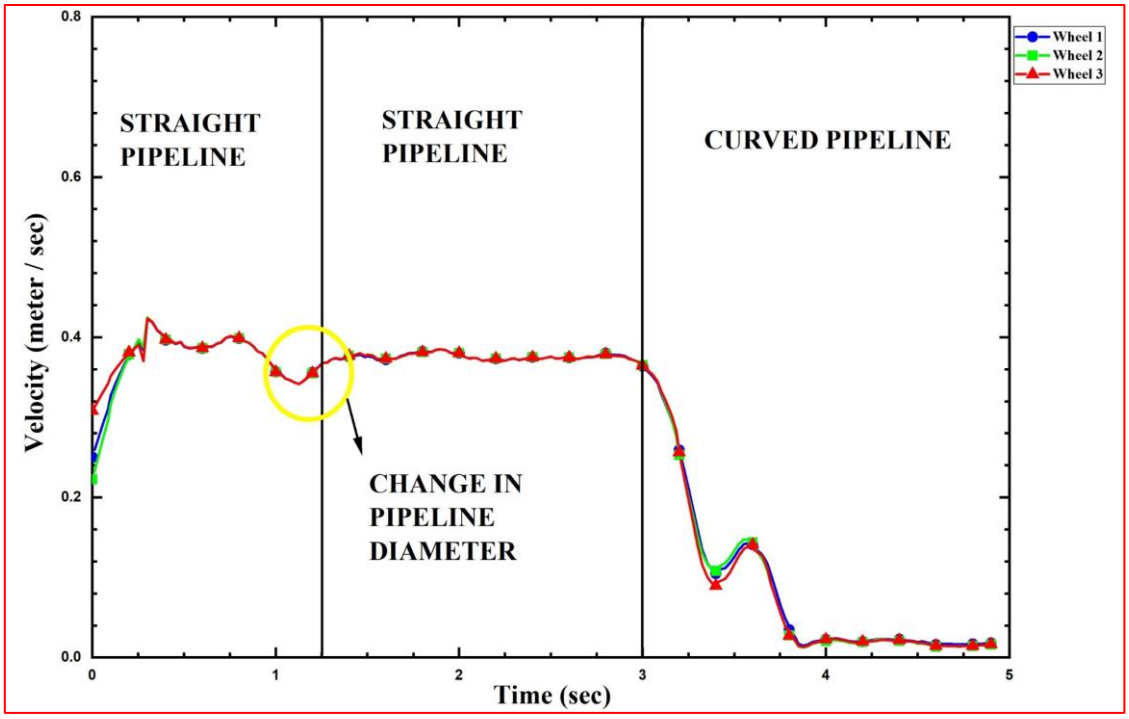

Fig. 15. The velocity of the robot when travelling in straight, curved and varying diameter pipeline

B. Modified design of wheeled IPIR

The proposed wheeled type In-Pipe Inspection Robot mounts the wheels asymmetrically at different angles. The placement of wheels produces an angle of 120°, 104.88° and 135.12° away from each other. The angle is calculated between the centres of each wheel from the central axis of the robot body. Fig. 16 shows the simulation environment and the proposed wheeled IPIR parameters.

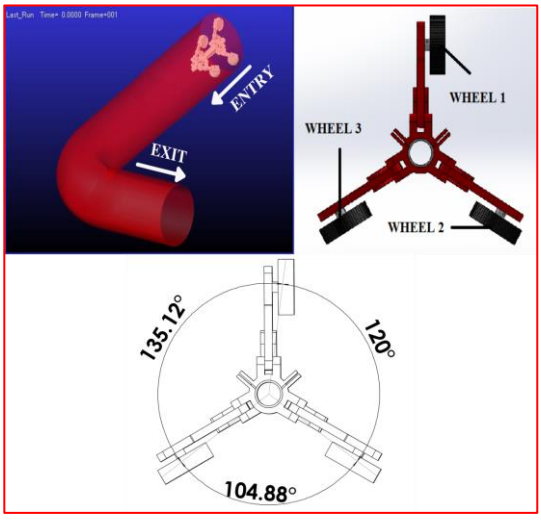

Fig. 16. Simulation environment and parameters used for the modified design of wheeled IPIR

1) Robot in the curved pipeline (Turning Left)

Fig. 17 displays the simulation result, which revealed that the robot wheels are always in touch with the inner pipeline surface. It employs the exact mechanism as a traditional wheeled type robot, except for the wheel mounting angle. As a result, the proposed design avoids the motion singularity in the curved pipeline (Left).

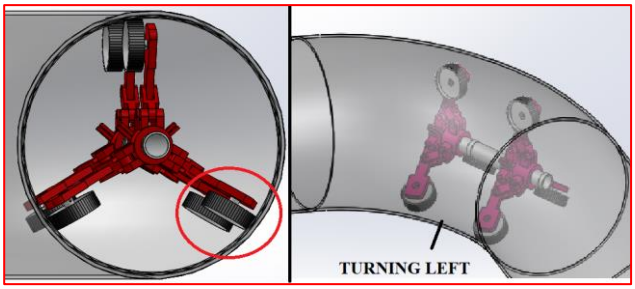

Fig. 17. Motion planning of robot in the curved pipeline (Turning Left) without singularity

Fig. 18 shows the angular velocity of wheels for the proposed robot. When the robot passes through a straight pipeline having a 350 mm inner diameter, the angular velocity of all three wheels remains constant. Little spikes in angular velocity were found when the inner pipeline diameter decreased to 340 mm. Then it travels through a straight pipeline where the three wheels' angular velocity remains constant. When the robot travels inside the curved pipeline, the wheel 3 angular velocity increases while the angular

velocity of wheels 1 and 2 decreases. Wheel 3 angular velocity increases because it passes through the concave part, and thus it has a high magnitude compared to the other two wheels. This shows that the robot's wheels are touching the surface while passing through the curved pipe. After it exits the curved pipe, it goes inside a straight pipeline where the angular velocity of the three wheels remains constant.

Fig. 19 shows the force acting on the wheels of the robot. It shows that the forces acting on all three wheels increases when it passes the curved pipeline. The forces acting on all three wheels are equal, with the forces ranging from 2.5-10 N.

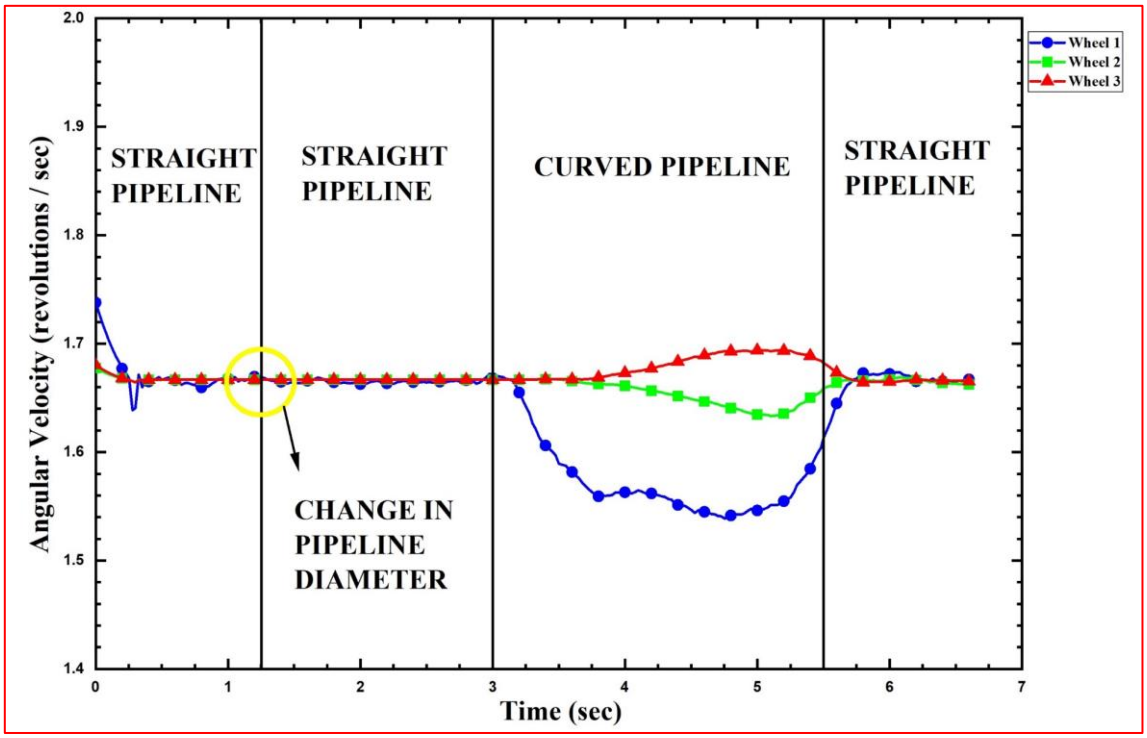

Fig. 18. Angular velocity of proposed robot wheels when passing through straight, curved (Turning Left) and varying diameter pipeline

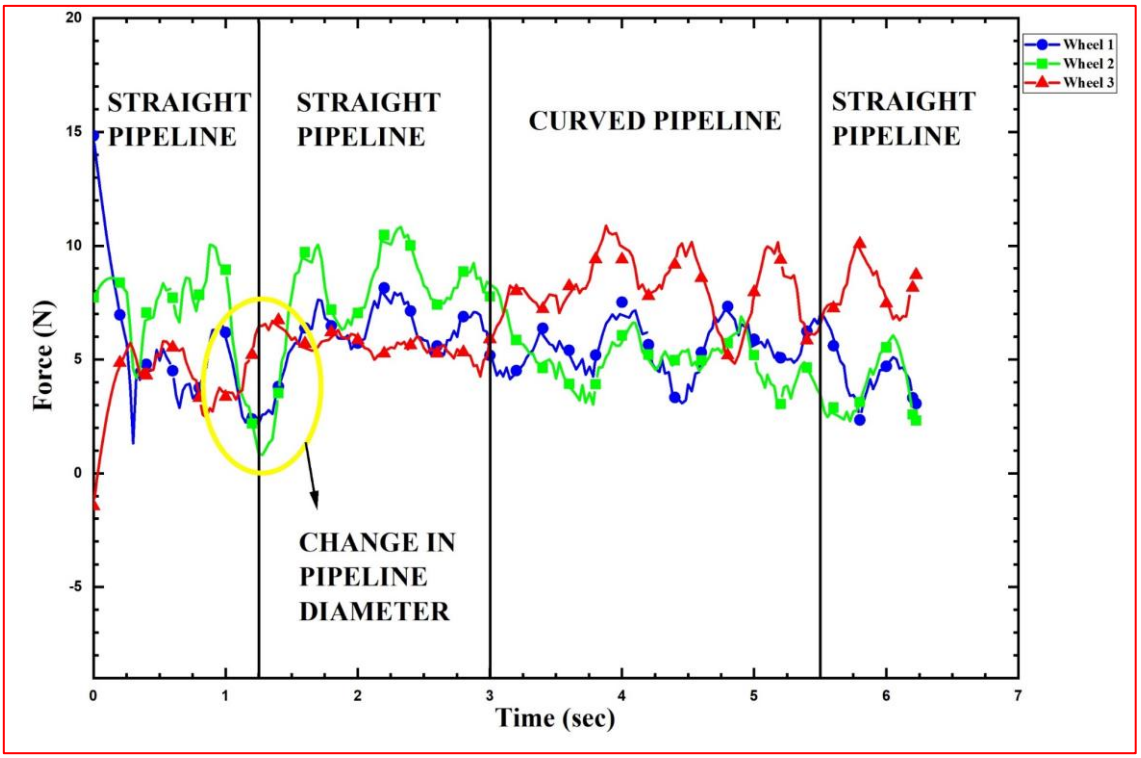

Fig. 19. Force acting on wheels of the proposed robot when passing through straight, curved (Turning Left) and varying diameter pipeline

Fig. 20 shows the spring force of the robot while travelling inside the pipeline. Spring 1 and 2 is the spring used in the front and back of the robot. Spring 1 gives a force of 11 N when passing through a straight pipe with an inner diameter of 350 mm. Spring 1 force increases to 17.25 N when the inner diameter of the pipe decreases to 340 mm. Spring 1 exerts a force of 15.65 N when the robot passes through the curved pipe. After exiting the curved pipe, it again enters the straight giving the same spring 1 force of 17.25 N. The same trend is followed by spring 2 as it passes the pipeline.

Fig. 21 shows the velocity of the proposed robot when passing through the pipeline. When travelling inside a straight pipeline with an inner diameter of 350 mm, the robot has a linear velocity of 0.39 m/sec. Then when the inner diameter changes to 340 mm, it has a linear velocity of 0.36 m/sec. When it passes through the curved pipeline wheel 1 and 2, velocity decreases as it is close to the convex part of the pipe. The wheel 3 velocity increases as it passes through the concave part of the curve pipe. As it re-enters the straight pipeline, its velocity returns to 0.36 m/sec. It maintains this constant velocity till it comes out of the pipeline. Since the velocity of the robot cannot be taken directly as the three wheels have different magnitudes at the curved pipelines. The robot travels at an average speed of 0.33 m/s through the straight and curved pipeline.

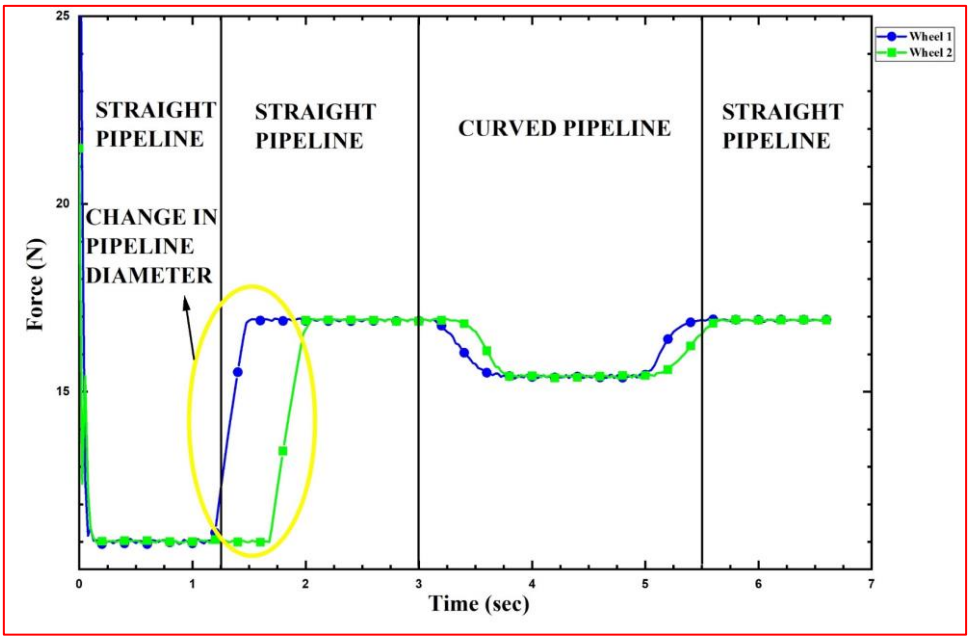

Fig. 20. Spring forces of the proposed robot when travelling inside straight, curved (Turning Left) and varying diameter pipeline

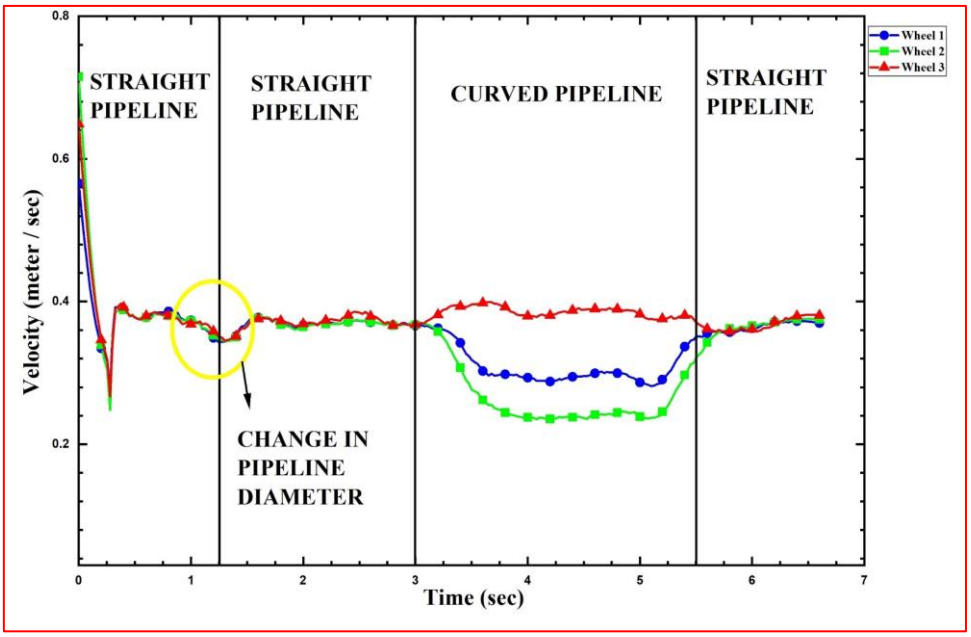

Fig. 21. The velocity of the proposed robot when travelling inside straight, curved (Turning Left) and varying diameter pipeline

2) Robot in the curved pipeline (Turning Right)

Fig. 22 depicts the robot's simulation result when passing through a curved pipeline (Right), and it shows that the proposed robot avoids motion singularity.

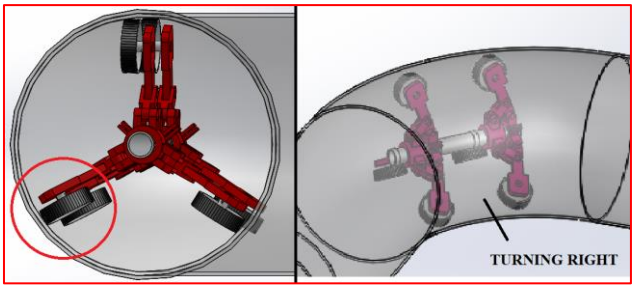

Fig. 22. Motion planning of robot in the curved pipeline (Turning Right) without singularity

Fig. 23 shows the angular velocity of the proposed robot. It shows that the angular velocity remains constant for all three wheels while travelling inside a straight pipeline with an inner diameter of 350 mm. This was still the same even when the inner diameter was decreased to 340 mm. After leaving the straight pipeline, it then joins the curved pipeline (Right). As it moves through the concave section of the pipeline, the angular velocity of wheels 1 and 2 increases. At the same time, wheel 3 angular velocity decreases as it moves through the convex part of the pipeline. The fact that wheel 2 angular velocity increased indicates that the wheel was in contact with the pipeline's inner surface, preventing motion singularity. It then passes through a straight pipeline after leaving the curved pipeline, where the angular velocity of all three wheels remains constant.

Fig. 24 shows the force acting on the robot's wheels. As the robot moves through the curved pipeline, the forces acting on all three wheels increase. The forces acting on all three wheels are more or less equal, with the forces ranging from 2.5 N to 12 N.

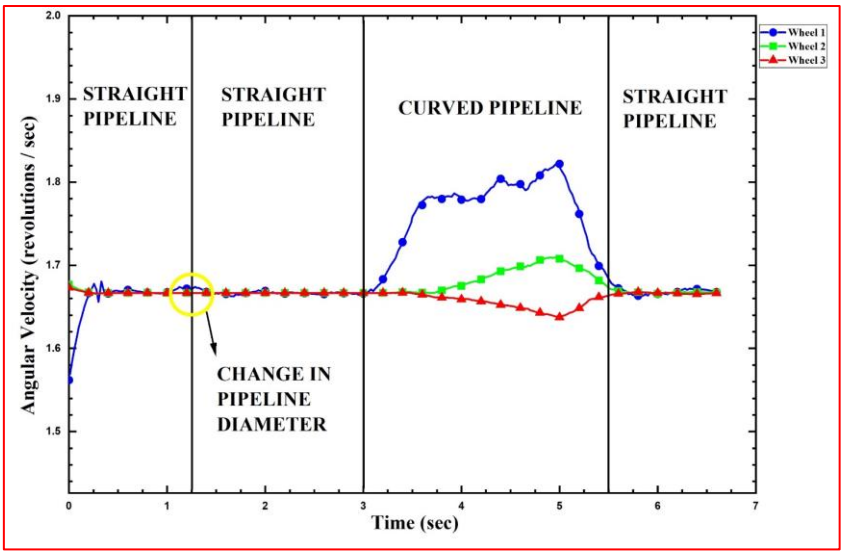

Fig. 23. Angular velocity of wheels for the proposed robot when travelling inside straight, curved (Turning Right) and varying diameter pipeline

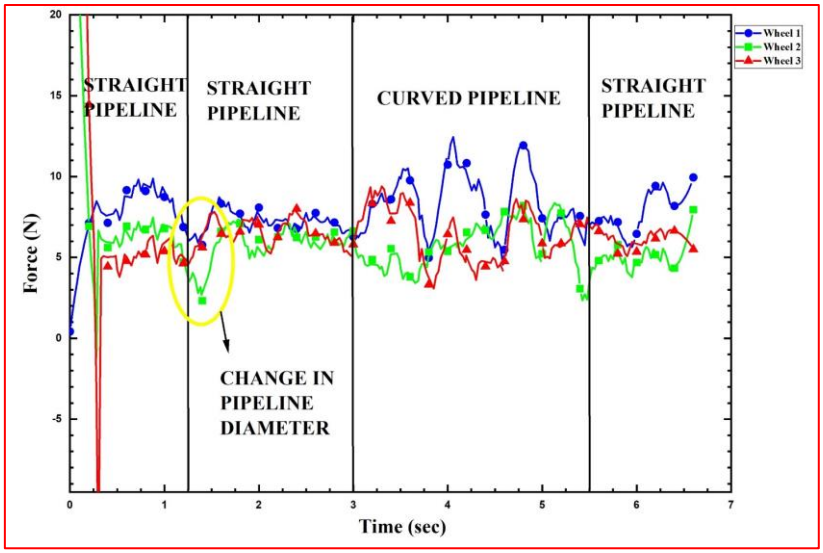

Fig. 24. Force acting on wheels of the proposed robot when passing through straight, curved (Turning Right) and varying diameter pipeline

Fig. 25 shows the spring force of the robot while passing through the pipeline. The 11 N force of spring 1 remains constant while entering a pipeline having a 350 mm inner diameter. Spring 1 force increases to 17.25 N as the inner diameter of the pipeline reduces to 340 mm. Then while travelling inside the curved pipeline, the spring 1 force reduces to 15.5 N, and when entering the straight pipeline again, the force increases by going back to 17.25 N. This same force trend is followed by spring 2 as it passes through the pipeline.

Fig. 26 shows the velocity of the robot while passing through the pipeline. When the robot passes the straight pipeline with an inner diameter of 350 mm, it has a velocity of 0.39 m/sec. When the inner diameter of the robot reduces to 340 mm, it has a velocity of 0.36 m/sec. When it passes through the curved pipeline, the velocity of wheels 1 and 2 increases with a decrease in wheel 3. This increase and decrease are because wheel 2 passes through the concave part, and wheel 3 passes through the convex part of the pipeline. The robot's velocity returns to 0.36 m/sec while entering the straight pipeline. The robot's average velocity while travelling inside the straight and curved pipeline was 0.33 m/sec.

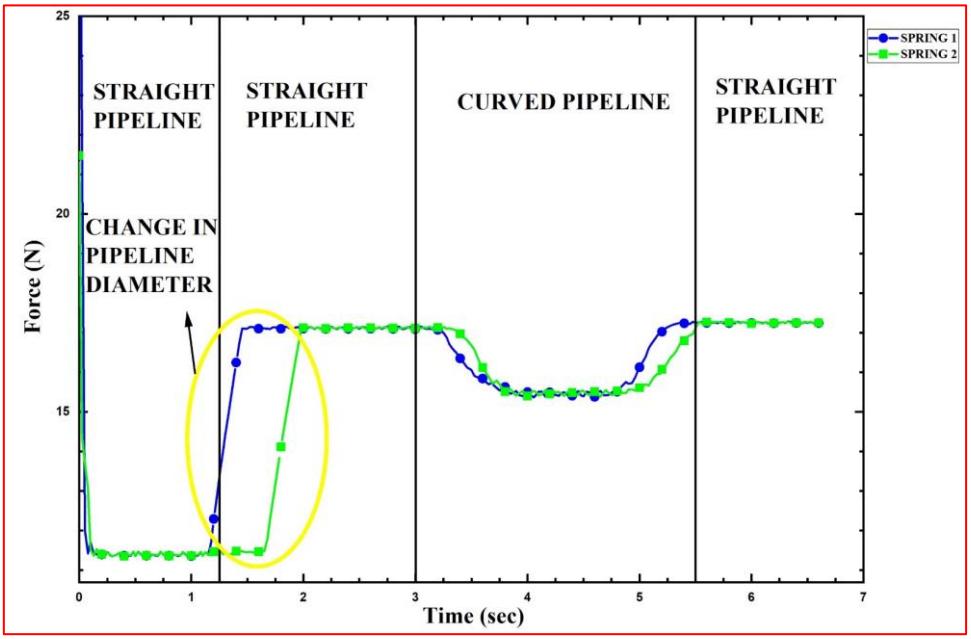

Fig. 25. Springs force of the proposed robot when travelling inside straight, curved (Turning Right) and varying diameter pipeline

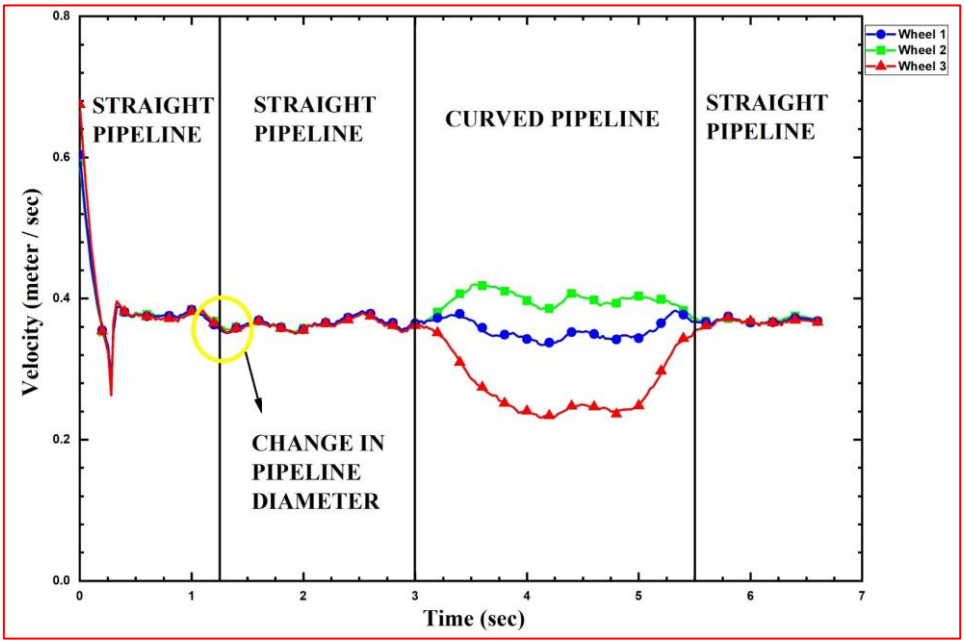

Fig. 26. The velocity of the proposed robot when travelling inside a straight, curved (Turning Right) and varying diameter pipeline

The advantages of the proposed robot over the Wheeled IPIR concerning motion singularity are summarized in Table 1.

TABLE I. COMPARISON BETWEEN WHEELED AND PROPOSED IPIR

Parameters	Wheeled IPIR	Proposed IPIR
Angular Velocity of wheel	Wheel 3 angular velocity at the concave part is lesser in magnitude	Wheel 3 angular velocity has a higher magnitude at the concave part
Forces acting on wheels	The reaction force acting on all the wheels are not uniform	The reaction force acting on all the wheels are uniform
Spring Force	The spring 2 force differs from the spring 1 force	The spring 2 force follows the same trend as the spring 1 force
Robot Velocity	The linear velocity of the robot at a straight pipeline is 0.35 m/s	The average linear velocity of the robot at both straight and curved pipelines is 0.33 m/s

IV. DEVELOPMENT OF PROTOTYPE

The modular parts designed using Solidworks software were printed using 3D printing technology. The parts that were 3D printed are the legs, tiny links, fixed joints and prismatic joints, as shown in Fig. 27. It also shows the assembled prototype of the robot. The material used for 3D printing was Polylactic Acid (PLA) filament which reduces the robot's weight without compromising its strength. The necessary force to push the legs is given by springs having 2.826 N/mm stiffness. Rubber wheels provide high friction between the wheel and the pipe surface—a DC motor of 100 rpm powers the wheels. The total weight of the robot is 1.6 kg, and the length is 300 mm. Any pipeline can use the developed IPIR, but only when there is no medium present inside the pipeline. Fig. 28 shows the experimental setup for studying the robot's motion inside the pipeline.

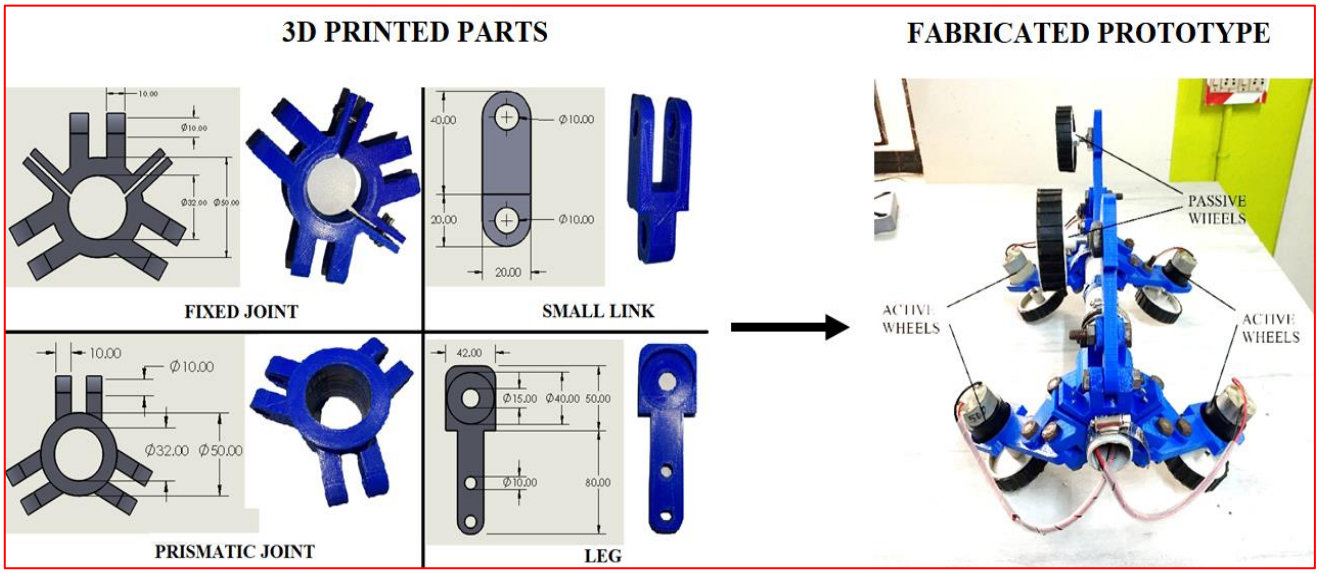

Fig. 27. Fabrication of IP-IR components through 3-D printing and Final Assembled IPIR

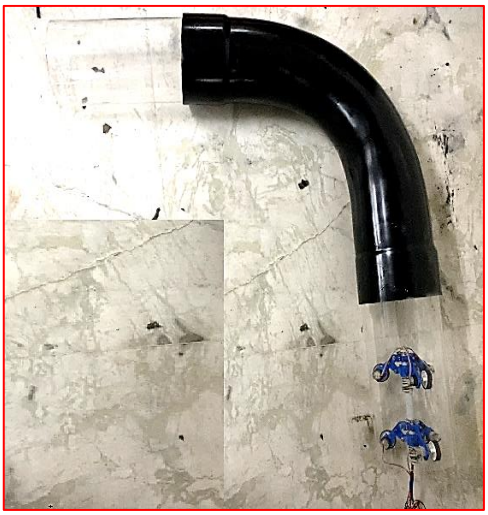

Fig. 28. Robot moving through the experimental setup

V. EXPERIMENTAL VERIFICATION

The robot was designed to enter a straight, curved and then exit a straight pipeline. The movement of the robot in the straight and curved pipeline (Turning left) was observed using a vision camera. It was found that the developed prototype avoids motion singularity at a curved pipeline. Fig. 29 shows the entry and exit of the robot, avoiding motion singularity.

In this experiment, the robot runs inside a straight pipeline, enters a curved pipeline (Turning right) and exists through a straight pipeline. The inner diameter of the straight and curved pipeline is 300 mm.

A DC motor using a Quadrature Encoder with an rpm of 110 is used to find the wheel velocity of the robot when travelling inside the straight and curved pipeline. This built-in encoder motor rotates and this produces pulses. These pulses alternate between high- and low-voltage electrical signals. A signal is said to be a single pulse when it transitions from low to high. When the motor makes a single 360-degree rotation, it generates a distinct pulse value. Ticks, another name for this pulse value, differ for each motor. The encoder motor we use has an 11 pulse per revolution (PPR). Then with the help of pulses, we can find the angular velocity of the motor using a micro-controller. Then using the angular velocity, we can find the linear velocity of the wheel using the following equation:

$$v = r * \omega \quad (7)$$

Where, r is the radius of the wheel in meters, ω is the angular velocity in radians per second and v is the linear velocity in meter per second.

Fig. 30 shows the velocity of the developed robot while passing through the pipeline. The results show a rise in velocity when wheel 2 passes through the concave part of the pipeline. Wheel 1 and 3 velocity decreases as it passes through the convex part of the pipeline. This decrease shows that all the wheels are in contact with the pipeline surface while passing through the curved pipeline. Thus, a change in wheel placement serves as a better solution against motion singularity. Table 2 shows the list of symbols used in this paper.

VI. CONCLUSIONS

In this paper, we have compared the existing model of wheeled type IPIR with the proposed wheeled type IPIR. The existing model mounts the three wheels at a 120° angle apart from each other. Simulations are performed for both the traditional and proposed wheeled type IPIR. Table 1 clearly displays the results from the simulation that placing the wheels at different angles avoids motion singularity instead of the 120° angle. The optimum angles are 120°, 104.88°, and 135.12°. Velocity and force analysis results for each wheel show how this design creates contact between the wheels and pipelines. The robot with the wheel mounting angle of 120° has an uneven force acting on the wheels while passing through the curved pipeline, and this was not the case for the developed robot. It also shows that the torque distribution in all the wheel motors is uniform due to the change in wheel position.

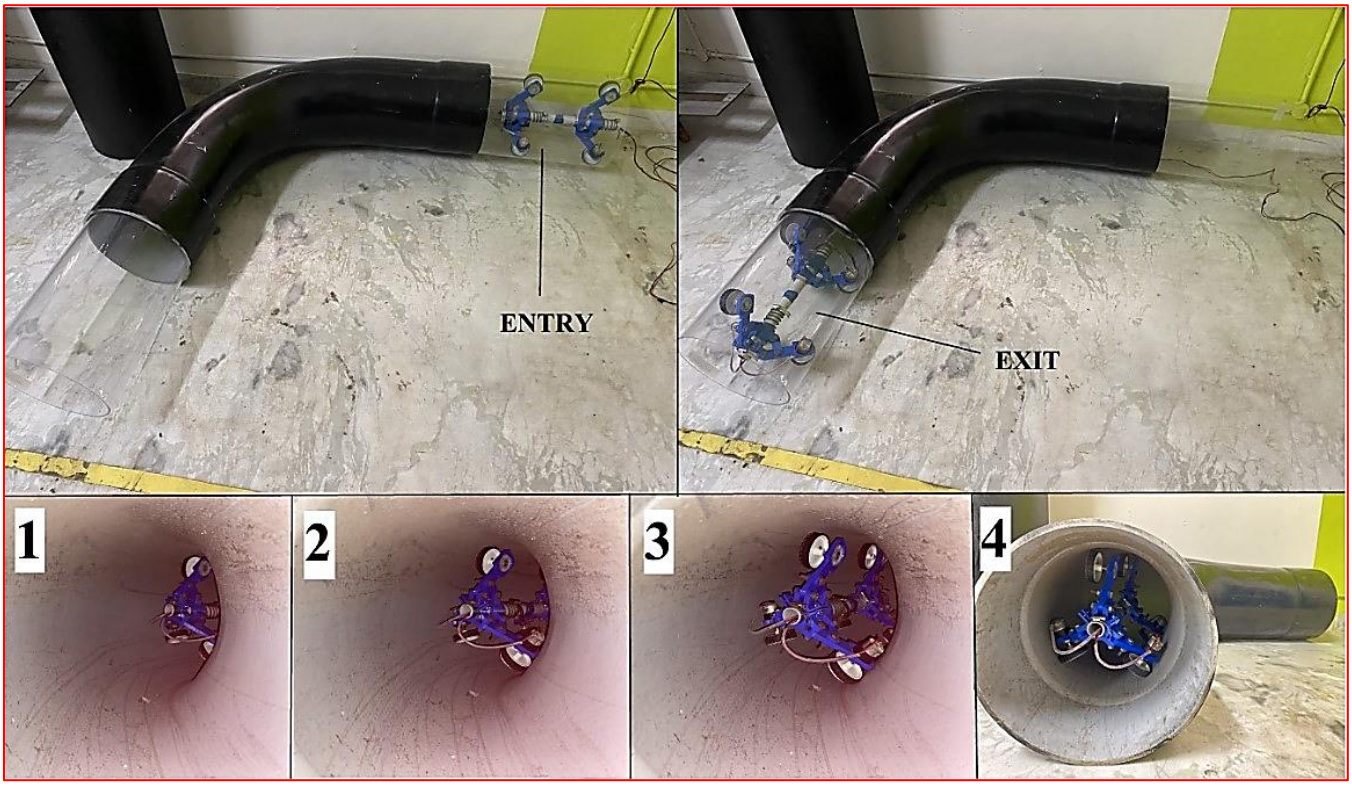

Fig. 29. Robot motion inside straight and curved pipeline avoiding motion singularity

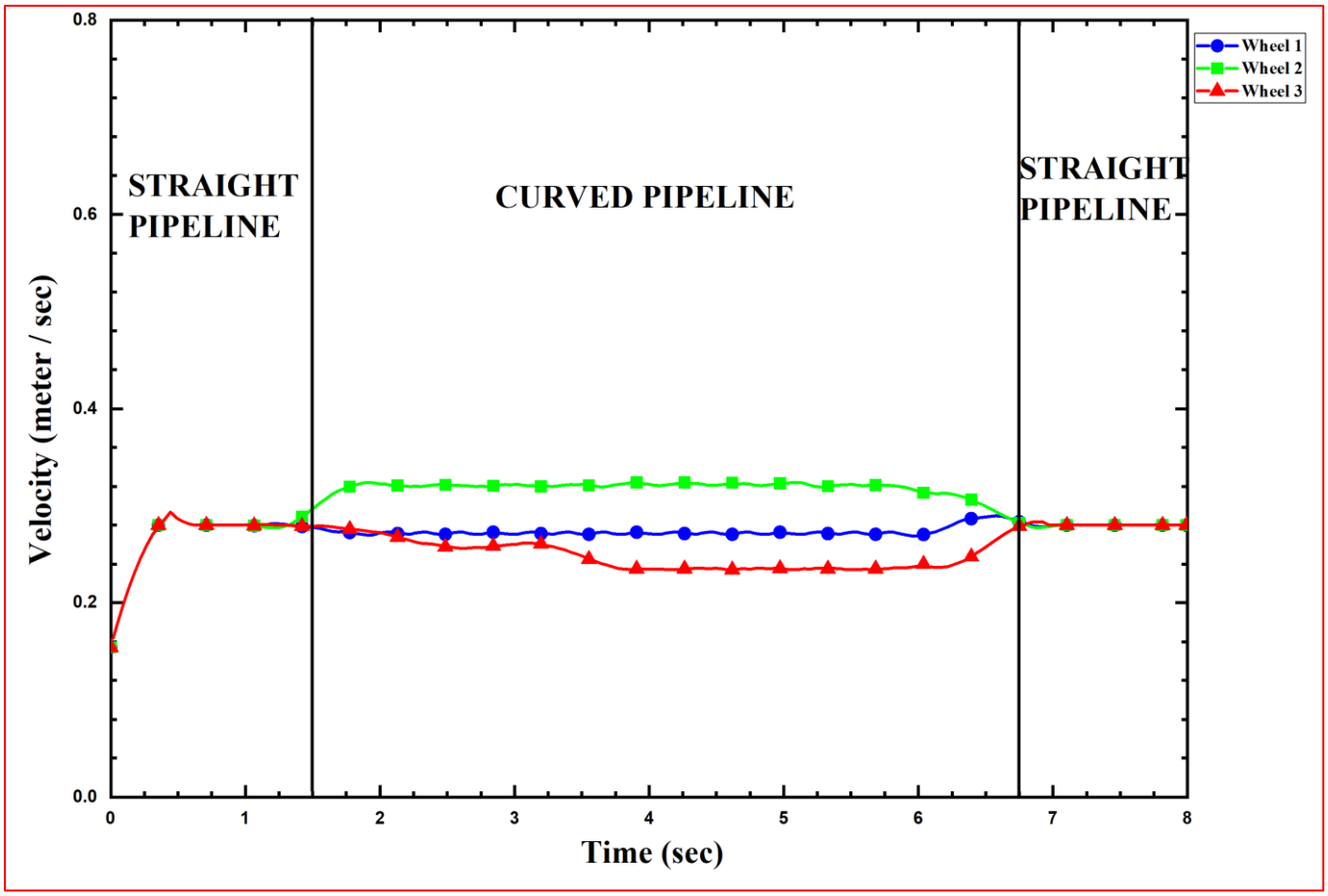

Fig. 30. The velocity of the robot when travelling inside a straight and curved pipeline (Turning right)

The choice of design parameters and motion constraints employed in the literature makes it difficult to compare it to the model that was previously available and reported in the literature.

There are no quantitative results from earlier research studies; only qualitative results are presented. It is very difficult to compare quantitatively with the prior results when looking at qualitative results. however, we can infer from the findings that our model is able to navigate curved pipelines avoiding motion singularity.

The simulation results were verified experimentally by letting the robot run inside a straight and curved pipeline. An encoder motor is used to create a velocity graph, which shows that the wheels never slip and are constantly in contact with the pipeline's inner surface. Experiments observed that the robot could pass through curved pipelines without motion singularity. The developed robot can run inside pipelines having an inner diameter of 250mm to 350 mm.

The robot is limited to moving in the horizontal plane and should be modified in future to move inside vertical pipes.

TABLE I. LIST OF SYMBOLS

Symbols	Full Form
F_{NZ}	Normal force acting on the wheel
F_{NX}	The traction force of the wheel
F_{JX}, F_{JZ}	Reaction forces acting at fixed joint
F_{SX}	Spring force
F_{SZ}	Reaction forces acting at prismatic joint
ℓ	Link length
θ	Angle symbol
m	Metre
mm	Millimetre
NDT	Non-Destructive Testing
IPIR	In-Pipe Inspection Robot
PIG	Pipeline Inspection Gauge
W	Total Weight of The Robot
r	The radius of The Wheel
3D	Three Dimensional
N	Newton
N/mm	Newton per Millimeter
Kg	Kilogram
Kg-cm	Kilogram Centimeter
°	Degree symbol
τ	Torque
∂	Partial differential symbol
rpm	Revolutions per minute
sec	Seconds
m/s	Meter per second
PLA	Polylactic Acid
DC	Direct Current

REFERENCES

[1] M. A. Adegboye, W. K. Fung, and A. Karnik, "Recent advances in pipeline monitoring and oil leakage detection technologies: Principles and approaches," *Sensors (Switzerland)*, vol. 19, no. 11, 2019, doi: 10.3390/s19112548.

[2] A. A. Carvalho, J. M. A. Rebello, M. P. V. Souza, L. V. S. Sagrilo, and S. D. Soares, "Reliability of non-destructive test techniques in the inspection of pipelines used in the oil industry," *International Journal of Pressure Vessels and Piping*, vol. 85, no. 11. 2008. doi: 10.1016/j.ijpvp.2008.05.001.

[3] A. Kakogawa and S. Ma, "Robotic Search and Rescue through In-Pipe Movement," in *Unmanned Robotic Systems and Applications*, 2020. doi: 10.5772/intechopen.88414.

[4] J. Zhou, T. Deng, J. Peng, G. Liang, X. Zhou, and J. Gong, "Experimental study on pressure pulses in long-distance gas pipeline during the pigging process," *Sci. Prog.*, vol. 103, no. 1, 2020, doi: 10.1177/0036850419884452.

[5] H. Zhang, J. Dong, C. Cui, and S. Liu, "Stress and strain analysis of spherical sealing cups of fluid-driven pipeline robot in dented oil and gas pipeline," *Eng. Fail. Anal.*, vol. 108, p. 104294, 2020, doi: 10.1016/j.engfailanal.2019.104294.

[6] C. Liu, Y. Wei, Y. Cao, S. Zhang, and Y. Sun, "Traveling ability of pipeline inspection gauge (PIG) in elbow under different friction coefficients by 3D FEM," *J. Nat. Gas Sci. Eng.*, vol. 75, no. December 2019, p. 103134, 2020, doi: 10.1016/j.jngse.2019.103134.

[7] J. Jiang, H. Zhang, B. Ji, F. Yi, F. Yan, and X. Liu, "Numerical investigation on sealing performance of drainage pipeline inspection gauge crossing pipeline elbows," *Energy Sci. Eng.*, vol. 9, no. 10, 2021, doi: 10.1002/ese3.955.

[8] J. Dong, S. Liu, H. Zhang, and H. Xiao, "Experiment and simulation of a controllable multi-airbag sealing disc of pipeline inspection gauges (PIGs)," *Int. J. Press. Vessel. Pip.*, vol. 192, 2021, doi: 10.1016/j.ijpvp.2021.104422.

[9] Z. Chen, "Deformation and stress analysis of cup on pipeline inspection gauge based on reverse measurement," *Energy Sci. Eng.*, no. January, pp. 2509–2526, 2022, doi: 10.1002/ese3.1241.

[10] H. Zhang, M. Q. Gao, B. Tang, C. Cui, and X. F. Xu, "Dynamic characteristics of the pipeline inspection gauge under girth weld excitation in submarine pipeline," *Pet. Sci.*, vol. 19, no. 2, 2022, doi: 10.1016/j.petsci.2021.09.044.

[11] T. Ren, Y. Zhang, Y. Li, Y. Chen, and Q. Liu, "Driving mechanisms, motion, and mechanics of screw drive in-pipe robots: A review," *Appl. Sci.*, vol. 9, no. 12, 2019, doi: 10.3390/app9122514.

[12] H. Tourajizadeh, V. Boomeri, M. Rezaei, and A. Sedigh, "Dynamic Optimization of a Steerable Screw In-pipe Inspection Robot Using HJB and Turbine Installation," *Robotica*, vol. 38, no. 11, 2020, doi: 10.1017/S0263574719001784.

[13] T. Li, K. Liu, H. Liu, X. Cui, B. Li, and Y. Wang, "Rapid design of a screw drive in-pipe robot based on parameterized simulation technology," *Simulation*, vol. 95, no. 7, 2019, doi: 10.1177/0037549718799881.

[14] H. Tourajizadeh, M. Rezaei, and A. H. Sedigh, "Optimal Control of Screw In-pipe Inspection Robot with Controllable Pitch Rate," *J. Intell. Robot. Syst. Theory Appl.*, vol. 90, no. 3–4, 2018, doi: 10.1007/s10846-017-0658-7.

[15] P. Li, M. Tang, C. Lyu, M. Fang, X. Duan, and Y. Liu, "Design and analysis of a novel active screw-drive pipe robot," *Adv. Mech. Eng.*, vol. 10, no. 10, 2018, doi: 10.1177/1687814018801384.

[16] Q. Tu, Q. Liu, T. Ren, and Y. Li, "Obstacle crossing and traction performance of active and passive screw pipeline robots," *J. Mech. Sci. Technol.*, vol. 33, no. 5, 2019, doi: 10.1007/s12206-019-0440-9.

[17] H. Tourajizadeh and M. Rezaei, "Design and control of a steerable screw in-pipe inspection robot," In 2016 4th International Conference on Robotics and Mechatronics (ICROM), pp. 98-104. IEEE, 2016. doi: 10.1109/ICRoM.2016.7886824.

[18] T. Yamamoto, S. Sakama, and A. Kamimura, "Pneumatic Duplex-Chambered Inchworm Mechanism for Narrow Pipes Driven by only Two Air Supply Lines," *IEEE Robot. Autom. Lett.*, vol. 5, no. 4, pp. 5034–5042, 2020, doi: 10.1109/LRA.2020.3003859.

[19] K. Kusunose *et al.*, "Development of inchworm type pipe inspection robot using extension type flexible pneumatic actuators," *Int. J. Automot. Mech. Eng.*, vol. 17, no. 2, pp. 8019–8028, 2020, doi: 10.15282/ijame.17.2.2020.20.0601.

[20] K. Hayashi *et al.*, "Improvement of pipe holding mechanism and inchworm type flexible pipe inspection robot," *Int. J. Mech. Eng. Robot. Res.*, vol. 9, no. 6, 2020, doi: 10.18178/ijmerr.9.6.894-899.

[21] D. Fang, J. Shang, Z. Luo, P. Lv, and G. Wu, "Development of a novel self-locking mechanism for continuous propulsion inchworm in-pipe robot," *Adv. Mech. Eng.*, vol. 10, no. 1, 2018, doi: 10.1177/1687814017749402.

[22] M. B. Khan *et al.*, "ICrawl: An Inchworm-Inspired Crawling Robot," *IEEE Access*, vol. 8, 2020, doi: 10.1109/ACCESS.2020.3035871.

[23] M. Aliff *et al.*, "Development of Pipe Inspection Robot using Soft Actuators, Microcontroller and LabVIEW," *Int. J. Adv. Comput. Sci. Appl.*, vol. 13, no. 3, pp. 349–354, 2022, doi: 10.14569/IJACSA.2022.0130343.

[24] J. Yang, Y. Xue, J. Shang, and Z. Luo, "Research on a new bilateral self-locking mechanism for an inchworm micro in-pipe robot with large traction," *Int. J. Adv. Robot. Syst.*, vol. 11, 2014, doi: 10.5772/59309.

[25] G. Feng, W. Li, Z. Li, and Z. He, "Development of a wheeled and wall-pressing type in-pipe robot for water pipelines cleaning and its traveling capability," *Mechanika*, vol. 26, no. 2, pp. 134–145, 2020, doi: 10.5755/j01.mech.26.2.18783.

[26] L. Brown, J. Carrasco, S. Watson, and B. Lennox, "Elbow Detection in Pipes for Autonomous Navigation of Inspection Robots," *J. Intell. Robot. Syst. Theory Appl.*, vol. 95, no. 2, 2019, doi: 10.1007/s10846-018-0904-7.

[27] L. Brown, J. Carrasco, and S. Watson, "Autonomous elbow controller for differential drive in-pipe robots," *Robotics*, vol. 10, no. 1, 2021, doi: 10.3390/robotics10010028.

[28] M. A. A. Wahed and M. R. Arshad, "Wall-press type pipe inspection robot," *In 2017 IEEE 2nd International Conference on Automatic Control and Intelligent Systems (I2CACIS), pp. 185-190. IEEE, 2017*, doi: 10.1109/I2CACIS.2017.8239055.

[29] H. Jang, T. Y. Kim, Y. C. Lee, Y. H. Song, and H. R. Choi, "Autonomous Navigation of In-Pipe Inspection Robot Using Contact Sensor Modules," *IEEE/ASME Trans. Mechatronics*, pp. 1–10, 2022, doi: 10.1109/TMECH.2022.3162192.

[30] S. Savin, S. Jatsun, and L. Vorochaeva, "State observer design for a walking in-pipe robot," *MATEC Web Conf.*, vol. 161, no. April, 2018, doi: 10.1051/matecconf/201816103012.

[31] S. Savin, "RRT-based Motion Planning for In-pipe Walking Robots," In 2018 Dynamics of Systems, Mechanisms and Machines (Dynamics), pp. 1-6. IEEE, 2018, doi: 10.1109/Dynamics.2018.8601473.

[32] G. H. Jackson-Mills *et al.*, "Non-assembly Walking Mechanism for Robotic In-Pipe Inspection," in *Lecture Notes in Networks and Systems*, 2022, vol. 324 LNNS. doi: 10.1007/978-3-030-86294-7_11.

[33] S. Savin and L. Vorochaeva, "Footstep planning for a six-legged in-pipe robot moving in spatially curved pipes," In 2017 International Siberian Conference on Control and Communications (SIBCON), pp. 1-6. IEEE, 2017, doi: 10.1109/SIBCON.2017.7998581.

[34] A. Zagler and F. Pfeiffer, "'MORITZ' a pipe crawler for tube junctions," *Proc. - IEEE Int. Conf. Robot. Autom.*, vol. 3, pp. 2954–2959, 2003, doi: 10.1109/robot.2003.1242044.

[35] W. Zhao, L. Zhang, and J. Kim, "Design and analysis of independently adjustable large in-pipe robot for long-distance pipeline," *Appl. Sci.*, vol. 10, no. 10, 2020, doi: 10.3390/app10103637.

[36] Z. Wu, Y. Wu, S. He, and X. Xiao, "Hierarchical fuzzy control based on spatial posture for a support-tracked type in-pipe robot," *Trans. Can. Soc. Mech. Eng.*, vol. 44, no. 1, 2020, doi: 10.1139/tcsme-2018-0052.

[37] M. Ciszewski, T. Buratowski, and M. Giergiel, "Modeling, Simulation and Control of a Pipe Inspection Mobile Robot with an Active Adaptation System," in *IFAC-PapersOnLine*, 2018, vol. 51, no. 22. doi: 10.1016/j.ifacol.2018.11.530.

[38] A. S. Z. Abidin *et al.*, "Development of In-Pipe Robot D300: Cornering Mechanism," in *MATEC Web of Conferences*, 2017, vol. 87. doi: 10.1051/matecconf/20178702029.

[39] V. Consumi, J. Merlin, L. Lindenroth, D. Stoyanov, and A. Stilli, "A Novel Soft Shape-shifting Robot with Track-based Locomotion for In-pipe Inspection," 2022, doi: https://arxiv.org/abs/2202.10840

[40] A. Hadi, A. Hassani, K. Alipour, R. Askari Moghadam, and P. Pourakbarian Niaz, "Developing an adaptable pipe inspection robot using shape memory alloy actuators," *J. Intell. Mater. Syst. Struct.*, vol. 31, no. 4, pp. 632–647, 2020, doi: 10.1177/1045389X19898255.

[41] H. Li, R. Li, J. Zhang, and P. Zhang, "Development of a pipeline inspection robot for the standard oil pipeline of china national petroleum corporation," *Appl. Sci.*, vol. 10, no. 8, 2020, doi: 10.3390/APP10082853.

[42] S. Kazeminasab and M. Kathrine Banks, "A Localization and Navigation Method for an In-pipe Robot in Water Distribution System through Wireless Control towards Long-Distance Inspection," *IEEE Access*, , 9, pp.117496-117511, 2021, doi: 10.1109/ACCESS.2021.3106880.

[43] R. S. Elankavi, D. Dinakaran, R. M. K. Chetty, M. M. Ramya, A. Selvakumar, and A. Doss, "Kinematic Modeling and Analysis of Wheeled In-Pipe Inspection Mobile Robot," In: Hussain C.M., Di Sia P. (eds) Handbook of Smart Materials, Technologies, and Devices. Springer, Cham, p p. 1–15, 2021, doi: 10.1007/978-3-030-58675-1_168-1.

[44] A. Kakogawa, Y. Komurasaki, and S. Ma, "Shadow-based operation assistant for a pipeline-inspection robot using a variance value of the image histogram," *J. Robot. Mechatronics*, vol. 31, no. 6, 2019, doi: 10.20965/jrm.2019.p0772.

[45] W. Zhao *et al.*, "A coordinated wheeled gas pipeline robot chain system based on visible light relay communication and illuminance assessment," *Sensors (Switzerland)*, vol. 19, no. 10, 2019, doi: 10.3390/s19102322.

[46] T.-J. Yeh and T.-H. Weng, "Analysis and Control of an In-Pipe Wheeled Robot With Spiral Moving Capability," *J. Auton. Veh. Syst.*, vol. 1, no. 1, 2021, doi: 10.1115/1.4048376.

[47] F. Yan, H. Gao, L. Zhang, and Y. Han, "Design and motion analysis of multi-motion mode pipeline robot," *J. Phys. Conf. Ser.*, vol. 2246, no. 1, 2022, doi: 10.1088/1742-6596/2246/1/012029.

[48] A. A. Bandala *et al*., "Control and Mechanical Design of a Multi-diameter Tri-Legged In- Pipe Traversing Robot," In 2019 IEEE/SICE International Symposium on System Integration (SII), pp. 740-745. IEEE, 2019, doi: 10.1109/SII.2019.8700363.

[49] H. Sawabe, M. Nakajima, M. Tanaka, K. Tanaka, and F. Matsuno, "Control of an articulated wheeled mobile robot in pipes," *Adv. Robot.*, vol. 33, no. 20, 2019, doi: 10.1080/01691864.2019.1666737.

[50] D. Zheng, H. Tan, and F. Zhou, "A design of endoscopic imaging system for hyper long pipeline based on wheeled pipe robot," *AIP Conf. Proc.*, vol. 1820, pp. 1–10, 2017, doi: 10.1063/1.4977316.

[51] E. Islas-garcía, M. Ceccarelli, R. Tapia-herrera, and C. R. Torres-sanmiguel, "Pipeline inspection tests using a biomimetic robot," *Biomimetics*, vol. 6, no. 1, pp. 1–16, 2021, doi: 10.3390/biomimetics6010017.

[52] M. Roussialian, H. Al Zanbarakji, A. Khawand, A. Rahal, and M. Owayjan, "Design and Development of a Pipeline Inspection Robot," *Mech. Mach. Sci.*, vol. 58, pp. 43–52, 2019, doi: 10.1007/978-3-319-89911-4_4.

[53] R. S. Elankavi, "Developments in Inpipe Inspectionrobot: a Review," *J. Mech. Contin. Math. Sci.*, vol. 15, no. 5, 2020, doi: 10.26782/jmcms.2020.05.00022.

[54] Y. Kwon and B. Yi, "Design and Motion Planning of a Two-Module," *IEEE Trans. Robot.*, vol. 28, no. 3, pp. 681–696, 2012, doi: 10.1109/TRO.2012.2183049.

[55] J. H. Kim, G. Sharma, and S. S. Iyengar, "FAMPER: A fully autonomous mobile robot for pipeline exploration," *Proc. IEEE Int. Conf. Ind. Technol.*, pp. 517–523, 2010, doi: 10.1109/ICIT.2010.5472748.

[56] Y. S. Kwon, B. Lee, I. C. Whang, W. K. Kim, and B. J. Yi, "A flat pipeline inspection robot with two wheel chains," *Proc. - IEEE Int. Conf. Robot. Autom.*, pp. 5141–5146, 2011, doi: 10.1109/ICRA.2011.5979712.

[57] M. S. Mohd Aras *et al., Design and development of remotely operated pipeline inspection robot*, In Proceedings of the 11th National Technical Seminar on Unmanned System Technology 2019, pp. 15-23, 2021, doi: 10.1007/978-981-15-5281-6_2.

[58] Y. Zhang and G. Yan, "In-pipe inspection robot with active pipe-diameter adaptability and automatic tractive force adjusting," *Mech. Mach. Theory*, vol. 42, no. 12, pp. 1618–1631, 2007, doi: 10.1016/j.mechmachtheory.2006.12.004.

[59] L. Xu, L. Zhang, J. Zhao, and K. Kim, "Cornering algorithm for a crawler in-pipe inspection robot," *Symmetry (Basel).*, vol. 12, no. 12, 2020, doi: 10.3390/sym12122016.

[60] E. N. P. M. K. N. Karuppasamy, "Defect identification in pipe lines using," *Int. J. Mech. Eng. Robot. Res.*, vol. 1, no. 2, pp. 19–31, 2012.

[61] W. C. Chang, Y. C. Huang, and P. Y. Chang, "Development of a 3D pipe robot for smart sensing and inspection using 3D printing technology," *Smart Sci.*, vol. 5, no. 3, 2017, doi: 10.1080/23080477.2017.1338428.

[62] R. S. Elankavi, D. Dinakaran, R. M. K. Chetty, and M. M. Ramya, "Mobility of Modular In-Pipe Inspection Robot inside Curved and L-Branch Pipes," *2021 IEEE Conf. Norbert Wiener 21st Century Being Hum. a Glob. Village, 21CW 2021*, 2021, doi: 10.1109/21CW48944.2021.9532536.